ON THE SOLUTION OF LAKE POLLUTION MODEL BY Sinc COLLOCATION METHOD

by

Turgut YELOGLU*

Department of Mathematics, Sinop University, Sinop, Turkey

Original scientific paper
https://doi.org/10.2298/TSCI2304385Y

In this paper, Sinc collocation method is employed for finding the approximate solution of the three lakes pollution model. In order to show the effectiveness and accuracy of the Sinc collocation method, several examples are presented in the tables and graphical forms. After observing the tables and graphical forms, it is concluded that Sinc collocation method is applicable with high accuracy to other real world problems.

Key words: *Sinc collocation method, lake pollution model, error estimation*

Introduction

Contamination in water resources that has various types such as thermal pollution, chemical pollution, radioactive pollution, *etc*., is an interesting topic in environmental sciences [1-10]. In [11], approximate solutions of the following model for pollution of three lakes have been studied by using Haar wavelet collocation method:

$$\begin{aligned}
\frac{\mathrm{d}p_1(t)}{\mathrm{d}t} &= \frac{F_{21}}{V_2}p_2(t) + \frac{F_{31}}{V_3}p_3(t) + f(t) - \frac{F_{12}}{V_1}p_1(t) - \frac{F_{13}}{V_1}p_1(t)\\
\frac{\mathrm{d}p_2(t)}{\mathrm{d}t} &= \frac{F_{12}}{V_1}p_1(t) + \frac{F_{32}}{V_3}p_3(t) - \frac{F_{21}}{V_2}p_2(t) - \frac{F_{23}}{V_2}p_2(t)\\
\frac{\mathrm{d}p_3(t)}{\mathrm{d}t} &= \frac{F_{13}}{V_1}p_1(t) + \frac{F_{23}}{V_2}p_2(t) - \frac{F_{32}}{V_3}p_3(t) - \frac{F_{31}}{V_3}p_3(t)
\end{aligned} \tag{1}$$

subject to the initial conditions:

$$p_1(0) = \lambda_1, \quad p_2(0) = \lambda_2, \quad p_3(0) = \lambda_3$$

where $p_i(t)$ for $i = 1, 2, 3$ are the amount of pollutant in lake i at time t, the rate of pollutant entering the 1st lake per unit time t is denoted by the function $f(t)$. The stream of water from i^{th} lake to j^{th} lake is denoted by F_{ij}. The V_i denotes the amount of the water in i^{th} lake. Differing from the results presented in [11], here we consider Sinc collocation method to find the approximate solutions of given model (1). To guarantee the constant amount of the water in each lake:

$$\begin{aligned}
F_{12} &= F_{21} + F_{31} + F_{13}\\
F_{23} &= F_{12} + F_{32} + F_{21}
\end{aligned} \tag{2}$$

conditions are assumed. For detailed information on Sinc collocation method, we refer the reader to [12-16].

* Author's, e-mail: turgutyeloglu@sinop.edu.tr

Preliminaries and notation

In this section, some preliminaries and notations related to sinc basis functions are given.

Definition 1. The Sinc function is defined on the whole real line $-\infty < x < \infty$ by:

$$\sin c(x) = \begin{cases} \dfrac{\sin(\pi x)}{\pi x} & x \neq 0 \\ 1 & x = 0 \end{cases}$$

Definition 2. For $h > 0$ and $k = 0, \pm 1, \pm 2, \ldots$ the translated Sinc function with space node are given by:

$$S(k,h)(x) = \sin c \frac{x-kh}{h} = \begin{cases} \dfrac{\sin\left(\pi \dfrac{x-kh}{h}\right)}{\pi \dfrac{x-kh}{h}} & x \neq kh \\ 1 & x = kh \end{cases}$$

Definition 3. If $f(x)$ is defined on the real line, then for $h > 0$ the series:

$$C(f,h)(x) = \sum_{k=-\infty}^{\infty} f(kh) \sin c\left(\frac{x-kh}{h}\right)$$

is called the Whittaker cardinal expansion of f whenever this series converges.

In general, approximations can be constructed for infinite, semi-infinite and finite intervals. To construct approximation on the interval (a, b) the conformal map

$$\phi(z) = \ln\left(\frac{z-a}{b-z}\right) \tag{3}$$

is employed. This map carries D_E the eye-shaped domain in the z-plane:

$$D_E = \left\{ z = x + iy: \quad \left|\arg\left(\frac{z-a}{b-z}\right)\right| < d \leq \frac{\pi}{2} \right\}$$

onto the infinite strip D_S:

$$D_S \equiv \left\{ w = u + iv : |V| < d \leq \frac{\pi}{2} \right\}$$

The basis functions on the interval (a, b) are derived from the composite translated sinc-functions:

$$S_k(z) = S(k,h)(z) o \phi(z) = \sin c\left(\frac{\phi(z) - kh}{h}\right)$$

for $z \in D_E$. The inverse map of $w = \phi(z)$ is:

$$z = \phi^{-1}(w) = \frac{a + be^w}{1 + e^w}$$

The sinc grid points $z_k \in (a, b)$ in D_E will be denoted by x_k because they are real. For the evenly spaced $\{kh\}_{k=-\infty}^{\infty}$ on the real line, the image which corresponds to these nodes is denoted by:

$$x_k = \phi^{-1}(kh) = \frac{a + be^{kh}}{1 + e^{kh}}, \quad k = 0, \pm 1, \pm 2, \ldots$$

Lemma 1. Let ϕ be the conformal one-to-one mapping of the simply connected domain D_E onto D_S, given by (2). Then:

$$\delta_{jk}^{(0)} = [S(j,h) o \phi(x)]|_{x=x_k} \begin{cases} 1 & j = k \\ 0 & j \neq k \end{cases}$$

$$\delta_{jk}^{(1)} = h \frac{\mathrm{d}}{\mathrm{d}\phi} [S(j,h) o \phi(x)]|_{x=x_k} \begin{cases} 0 & j = k \\ \dfrac{(-1)^{k-j}}{k-j} & j \neq k \end{cases}$$

$$\delta_{jk}^{(2)} = h_2 \frac{\mathrm{d}}{\mathrm{d}\phi} [S(j,h) o \phi(x)]|_{x=x_k} \begin{cases} -2^3 (-1)^{k-j} & j = k \\ (k-j)^2 & j \neq k \end{cases}$$

The sinc-collocation method

We assume approximate solutions for problem (1) with initial conditions by the finite expansion of Sinc basis functions:

$$p_{1,n}(x) = \sum_{k=-M}^{N} c_k x S_k(x), \quad n = M + N + 1$$

$$p_{2,n}(x) = \sum_{k=-M}^{N} d_k x S_k(x), \quad n = M + N + 1$$

$$p_{3,n}(x) = \sum_{k=-M}^{N} e_k x S_k(x), \quad n = M + N + 1$$

where $S_k(x)$ is the function $S(k, h) \circ \phi(x)$. Here, the unknown coefficients are determined by Sinc collocation method *via* the following theorem.

Theorem 1. Let be a function $f(x) = \Sigma_{k=-M}^{N} c_k x S_k(x)$ defined as the finite expansion of Sinc basis functions, then the first derivative of $f(x)$ is given by:

$$\frac{\mathrm{d}}{\mathrm{d}x} f(x) = \sum_{k=-M}^{N} c_k \left[x\phi'(x) \frac{\mathrm{d}}{\mathrm{d}\phi} S_k(x) + S_k(x) \right] \tag{4}$$

After the above theorem is applied to model (1), we obtain a linear algebraic equation system. By solving the system, it is calculated the unknown coefficients c_k, d_k, and e_k.

Error estimation

In this section, we use the estimated error function $\tilde{E}_N(x)$ to check the accuracy of the presented method. The estimated error function $\tilde{E}_N(x)$ might be used in the problems that are unknown the exact solutions. If the $p_{1,n}(x)$, $p_{2,n}(x)$, and $p_{3,n}(x)$ are an approximate solution to system (1), then when these functions and their derivatives are substituted into system (1)

the obtained equation should be satisfied approximately. In short, for $x_k \in [a, b]$, the functions $\tilde{E}_{i,N}(x)$, $i = 1, 2, 3$ are defined by:

$$\tilde{E}_{1,N}(x_k) = \left| p'_{1,n}(x_k) - \frac{F_{21}}{V_2} p_{2,n}(x_k) - \frac{F_{31}}{V_3} p_{3,n}(x_k) - f(x_k) + \frac{F_{12}}{V_1} p_{1,n}(x_k) + \frac{F_{13}}{V_1} p_{1,n}(x_k) \right| \cong 0$$

$$\tilde{E}_{2,N}(x_k) = \left| p'_{2,n}(x_k) - \frac{F_{12}}{V_1} p_{1,n}(x_k) - \frac{F_{32}}{V_3} p_{3,n}(x_k) + \frac{F_{21}}{V_2} p_{2,n}(x_k) + \frac{F_{23}}{V_2} p_{2,n}(x_k) \right| \cong 0$$

$$\tilde{E}_{3,N}(x_k) = \left| p'_{3,n}(x_k) - \frac{F_{13}}{V_1} p_{1,n}(x_k) - \frac{F_{23}}{V_2} p_{2,n}(x_k) + \frac{F_{32}}{V_3} p_{2,n}(x_k) + \frac{F_{31}}{V_3} p_{3,n}(x_k) \right| \cong 0$$

and $\tilde{E}_{i,N}(x) \le 10^{-t_k}$, $i = 1, 2, 3$ (t_k any positive contant). If $\max 10^{-t_k} = 10^{-t}$ is prescribed, the truncation limit N is increased until the difference $\tilde{E}_{i,N}(x_k), i = 1, 2, 3$ at each of the points becomes smaller than the prescribed 10^{-t}.

Numerical simulation and discussion

In this section, for different $f(t)$ functions, the numerical examples are presented to show the accuracy and efficiency of the proposed method. In the all examples, we choose the parameters as V_1 = 2900 km^3, V_2 = 850 km^3, V_3 = 1180 km^3, F_{12} = 24 km^3 per year, F_{13} = 22 km^3 per year, F_{21} = 14 km^3 per year, F_{23} = 18 km^3 per year, F_{31} = 32 km^3 per year, F_{32} = 8 km^3 per year. Also, the initial conditions are given by $p_1(0) = 0$, $p_2(0) = 0$, and $p_3(0) = 0$. In the all examples, we take $N = M$. As a result, regarding to the results in each table in the all examples, it is seen that the error of each result decrease significantly while the interpolation level N increases.

Example 1. We assume $f(t) = 100$ then the system model (1) turns into:

$$\begin{aligned} \frac{dp_1}{dt} &= \frac{14}{850} p_2(t) + \frac{32}{1180} p_3(t) + 100 - \frac{24}{2900} p_1(t) - \frac{22}{2900} p_1(t) \\ \frac{dp_2}{dt} &= \frac{24}{2900} p_1(t) + \frac{8}{1180} p_3(t) - \frac{14}{850} p_2(t) - \frac{18}{850} p_2(t) \\ \frac{dp_3}{dt} &= \frac{22}{2900} p_1(t) + \frac{18}{850} p_2(t) - \frac{32}{1180} p_3(t) - \frac{8}{1180} p_3(t) \end{aligned} \tag{5}$$

Numerical results for different N values for (5) are given in the tabs. 1-3. The graphics of the estimated error functions for N = 32 are presented in fig. 1.

Table 1. Numerical values of the estimated error function $\tilde{E}_{1,N}$ for *Example 1* for different values of N

x	$\tilde{E}_{1,16}$	$\tilde{E}_{1,32}$	$\tilde{E}_{1,64}$	$\tilde{E}_{1,128}$
0.2	5.52002×10^{-5}	1.29004×10^{-6}	1.39747×10^{-10}	5.34239×10^{-13}
0.4	2.69985×10^{-5}	8.76099×10^{-8}	3.87013×10^{-9}	3.97904×10^{-13}
0.6	2.70426×10^{-5}	8.76596×10^{-8}	3.87149×10^{-9}	3.94129×10^{-13}
0.8	5.54385×10^{-5}	1.29191×10^{-6}	1.39942×10^{-10}	5.52447×10^{-13}

Table 2. Numerical values of the estimated error function $\tilde{E}_{2,N}$ for *Example 1* for different values of *N*

x	$\tilde{E}_{2,16}$	$\tilde{E}_{2,32}$	$\tilde{E}_{2,63}$	$\tilde{E}_{2,128}$
0.2	2.87020×10^{-5}	6.70784×10^{-7}	7.26749×10^{-11}	2.79332×10^{-13}
0.4	1.40436×10^{-5}	4.55602×10^{-8}	2.01256×10^{-9}	2.10942×10^{-13}
0.6	1.40725×10^{-5}	4.55929×10^{-8}	2.01347×10^{-9}	2.04614×10^{-13}
0.8	2.88584×10^{-5}	6.72017×10^{-7}	7.27840×10^{-11}	2.86215×10^{-13}

Table 3. Numerical values of the estimated error function $\tilde{E}_{3,N}$ for *Example 1* for different values N

x	$\tilde{E}_{3,16}$	$\tilde{E}_{3,32}$	$\tilde{E}_{3,63}$	$\tilde{E}_{3,128}$
0.2	2.64982×10^{-5}	6.19252×10^{-7}	6.70880×10^{-11}	2.57572×10^{-13}
0.4	1.29545×10^{-5}	4.20497×10^{-8}	1.85756×10^{-9}	1.96287×10^{-13}
0.6	1.29700×10^{-5}	4.20668×10^{-8}	1.85803×10^{-9}	1.89515×10^{-13}
0.8	2.65801×10^{-5}	6.19896×10^{-7}	6.71552×10^{-11}	2.64400×10^{-13}

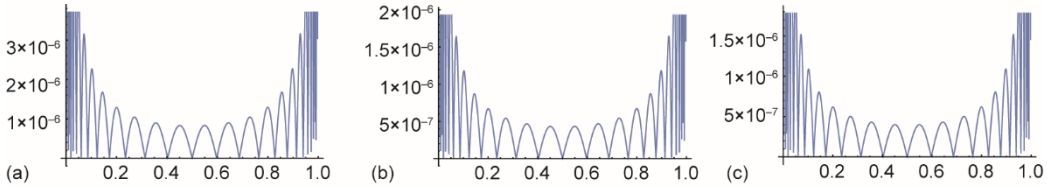

Figure 1. Graphical representation of the estimated error functions of *Example 1* for $N = 32$; (a) $\tilde{E}_{1,N}$, (b) $\tilde{E}_{2,N}$, and (c) $\tilde{E}_{3,N}$

Example 2. We assume $f(t) = 200e^{-10t}$ then the system model (1) turns into

$$\begin{aligned}
\frac{\mathrm{d}p_1}{\mathrm{d}t} &= \frac{14}{850}p_2(t) + \frac{32}{1180}p_3(t) + 200e^{-10t} - \frac{24}{2900}p_1(t) - \frac{22}{2900}p_1(t) \\
\frac{\mathrm{d}p_2}{\mathrm{d}t} &= \frac{24}{2900}p_1(t) + \frac{8}{1180}p_3(t) - \frac{14}{850}p_2(t) - \frac{18}{850}p_2(t) \\
\frac{\mathrm{d}p_3}{\mathrm{d}t} &= \frac{22}{2900}p_1(t) + \frac{18}{850}p_2(t) - \frac{32}{1180}p_3(t) - \frac{8}{1180}p_3(t)
\end{aligned} \tag{6}$$

Numerical results for different N values for (6) are given in the tabs. 4-6. The graphics of the estimated error functions for $N = 32$ are presented in fig. 2.

Table 4. Numerical values of the estimated error function $\tilde{E}_{1,N}$ for *Example* 2 for different values of *N*

x	$\tilde{E}_{1,16}$	$\tilde{E}_{1,32}$	$\tilde{E}_{1,63}$	$\tilde{E}_{1,128}$
0.2	1.25842×10^{-2}	3.06924×10^{-4}	3.21913×10^{-8}	1.25258×10^{-10}
0.4	6.60769×10^{-3}	2.09006×10^{-5}	8.90894×10^{-7}	9.19371×10^{-11}
0.6	6.93272×10^{-3}	2.08203×10^{-5}	8.91056×10^{-7}	9.09637×10^{-11}
0.8	1.44402×10^{-2}	3.04546×10^{-4}	3.22067×10^{-8}	1.26917×10^{-10}

Table 5. Numerical values of the estimated error function $\tilde{E}_{2,N}$ for *Example 2* for different values of *N*

x	$\tilde{E}_{2,16}$	$\tilde{E}_{2,32}$	$\tilde{E}_{2,63}$	$\tilde{E}_{2,128}$
0.2	8.11764×10^{-6}	2.13447×10^{-7}	2.32877×10^{-11}	9.33698×10^{-14}
0.4	5.04203×10^{-6}	1.63123×10^{-8}	6.97340×10^{-10}	7.23588×10^{-14}
0.6	6.38604×10^{-6}	1.85641×10^{-8}	7.67070×10^{-10}	7.67164×10^{-14}
0.8	1.50519×10^{-5}	2.97178×10^{-7}	2.96332×10^{-11}	1.12327×10^{-13}

Table 6. Numerical values of the estimated error function $\tilde{E}_{3,N}$ for *Example 2* for different values of *N*

x	$\tilde{E}_{3,16}$	$\tilde{E}_{3,32}$	$\tilde{E}_{3,63}$	$\tilde{E}_{3,128}$
0.2	7.53189×10^{-6}	1.97752×10^{-7}	2.15744×10^{-11}	8.64586×10^{-14}
0.4	4.66392×10^{-6}	1.50912×10^{-8}	6.45413×10^{-1}	6.69881×10^{-14}
0.6	5.89347×10^{-6}	1.71511×10^{-8}	7.09204×10^{-10}	7.08877×10^{-14}
0.8	1.38756×10^{-5}	2.74351×10^{-7}	2.73795×10^{-11}	1.03778×10^{-13}

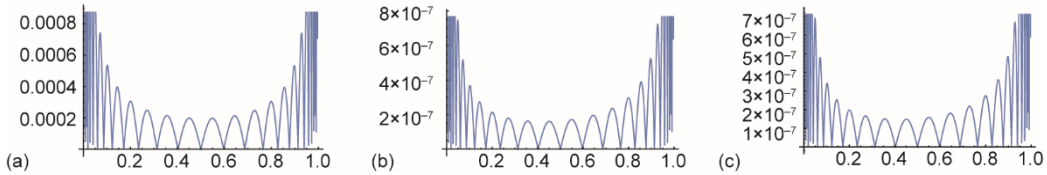

Figure 2. Graphical representation of the estimated error functions of *Example 2* for $N = 32$; (a) $\tilde{E}_{1,N}$, (b) $\tilde{E}_{2,N}$, and (c) $\tilde{E}_{3,N}$

Example 3. We assume $f(t) = 1 + \sin t$ then the system model (1) turns into:

$$\begin{aligned}
\frac{\mathrm{d}p_1}{\mathrm{d}t} &= \frac{14}{850}p_2(t) + \frac{32}{1180}p_3(t) + 1 + \sin t - \frac{24}{2900}p_1(t) - \frac{22}{2900}p_1(t) \\
\frac{\mathrm{d}p_2}{\mathrm{d}t} &= \frac{24}{2900}p_1(t) + \frac{8}{1180}p_3(t) - \frac{14}{850}p_2(t) - \frac{18}{850}p_2(t) \\
\frac{\mathrm{d}p_3}{\mathrm{d}t} &= \frac{22}{2900}p_1(t) + \frac{18}{850}p_2(t) - \frac{32}{1180}p_3(t) - \frac{8}{1180}p_3(t)
\end{aligned} \tag{7}$$

Numerical results for different N values for (7) are given in the tabs. 7-9. The graphics of the estimated error functions for $N = 32$ are presented in fig. 3.

Table 7. Numerical values of the estimated error function $\tilde{E}_{1,N}$ for *Example 3* for different values of *N*

x	$\tilde{E}_{1,16}$	$\tilde{E}_{1,32}$	$\tilde{E}_{1,63}$	$\tilde{E}_{1,128}$
0.2	3.06869×10^{-5}	7.37963×10^{-7}	8.02156×10^{-11}	3.06533×10^{-13}
0.4	1.50786×10^{-5}	5.01220×10^{-8}	2.22095×10^{-9}	2.33813×10^{-13}
0.6	1.53269×10^{-5}	5.01968×10^{-8}	2.22141×10^{-9}	2.25930×10^{-13}
0.8	3.20693×10^{-5}	7.41039×10^{-7}	8.02861×10^{-11}	3.15969×10^{-13}

Table 8. Numerical values of the estimated error function $\tilde{E}_{2,N}$ for *Example 3* for different values of *N*

x	$\tilde{E}_{2,16}$	$\tilde{E}_{2,32}$	$\tilde{E}_{2,63}$	$\tilde{E}_{2,128}$
0.2	3.79019×10^{-7}	8.91501×10^{-9}	9.64624×10^{-13}	3.68629×10^{-15}
0.4	1.79574×10^{-7}	6.00119×10^{-10}	2.65759×10^{-11}	2.81719×10^{-15}
0.6	1.74009×10^{-7}	5.93951×10^{-10}	2.64086×10^{-11}	2.68535×10^{-15}
0.8	3.48909×10^{-7}	8.68196×10^{-9}	9.49761×10^{-13}	3.74440×10^{-15}

Table 9. Numerical values of the estimated error function $\tilde{E}_{3,N}$ for *Example 2* for different values of *N*

x	$\tilde{E}_{3,16}$	$\tilde{E}_{3,32}$	$\tilde{E}_{3,63}$	$\tilde{E}_{3,128}$
0.2	7.53189×10^{-7}	1.97752×10^{-9}	2.15744×10^{-13}	8.64586×10^{-15}
0.4	4.66392×10^{-7}	1.50912×10^{-10}	6.45413×10^{-11}	6.69881×10^{-15}
0.6	5.89347×10^{-7}	1.71511×10^{-10}	7.09204×10^{-11}	7.08877×10^{-15}
0.8	1.38756×10^{-7}	2.74351×10^{-9}	2.73795×10^{-13}	1.03778×10^{-15}

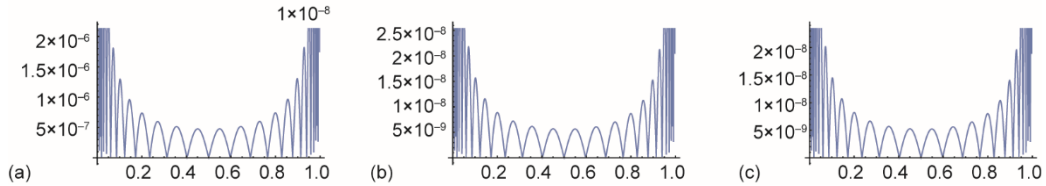

Figure 3. Graphical representation of the estimated error functions of *Example 3* for $N = 32$; (a) $\tilde{E}_{1,N}$, (b) $\tilde{E}_{2,N}$, and (c) $\tilde{E}_{3,N}$

Conclusion

In this paper, Sinc collocation method is applied to obtain an approximate solutions of model (1) with initial conditions. The model for different $f(t)$ functions are approximately solved and the estimated errors are presented using tables. The numerical results showed that the method is a powerful tool for solving the given model approximately.

References

[1] Sun, B. Y., Yang, X. H., The Input and Output Relationship of Water Resource in Jilin From 2004 to 2017, *Thermal Science, 24* (2020), 4, pp. 2337-2345
[2] Hasan, M. K., *et al*., Water Pollution in Bangladesh and Its Impact on Public Health, *Heliyon, 5* (2019), 8, e02145
[3] Zhou, Z., *et al*., Does the" 10-Point Water Plan" Reduce the Intensity of Industrial Water Pollution? Quasi-Experimental Evidence from China, *Journal of Environmental Management, 295* (2021), Oct., 113048
[4] Chen, Y. J., *et al*., Evaluation of Water Resource's Carrying Capacity Based on Three-Element Connection Number a Case Study of Beijing-Tianjin-Hebei Region, *Thermal Science, 27* (2023), 3A, pp. 2019-2027
[5] Yi, Z. J., *et al*., A Water Quality Prediction Model for Large-Scale Rivers Based on Projection Pursuit Regression in the Yangtze River, *Thermal Science, 26* (2022), 3B, pp. 2561-2567

[6] Rafiq, A., *et al*., Photocatalytic Degradation of Dyes Using Semiconductor Photocatalysts to Clean Industrial Water Pollution, *Journal of Industrial and Engineering Chemistry, 97* (2021), May, pp. 111-128
[7] Zamora-Ledezma, C., *et al*., Heavy Metal Water Pollution: A Fresh Look About Hazards, Novel and Conventional Remediation Methods, *Environmental Technology & Innovation, 22* (2021), May, 101504
[8] Chen, H., *et al*., A Deep Learning CNN Architecture Applied in Smart Near-Infrared Analysis of Water Pollution for Agricultural Irrigation Resources, *Agricultural Water Management, 240* (2020), Oct., 106303
[9] Ji, M., *et al*., Bacteriophages in Water Pollution Control: Advantages and Limitations, *Frontiers of Environmental Science & Engineering, 15* (2021), 84, pp. 1-15
[10] Iervolino, G., *et al*., Enhanced Removal of Water Pollutants by Dielectric Barrier Discharge Non-Thermal Plasma Reactor, *Separation and Purification Technology, 215* (2019), May, pp. 155-162
[11] Hatipoglu, V. F., A Novel Model for the Contamination of a System of Three Artificial Lakes, *Discrete and Continuous Dynamical Systems-S, 14* (2021), 7, pp. 2261-2272
[12] Hatipoglu, V. F., *et al*., An Efficient Scheme for Solving a System of Fractional Differential Equations with Boundary Conditions, *Advances in Difference Equations, 2017* (2017), 1, pp. 1-13
[13] Alkan, S., Approximate Solutions of Boundary Value Problems of Fractional Order by Using Sinc-Galerkin Method, *New Trends in Mathematical Sciences, 2* (2014), 1, pp. 1-11
[14] Alkan, S., A Numerical Method for Solution of Integro-Differential Equations of Fractional Order, *Sakarya University Journal of Science, 21* (2017), 2, pp. 82-89
[15] Hatipoglu, V. F., A Numerical Algorithm for the Solution of Non-Linear Fractional Differential Equations *via* Beta-Derivatives, (2019), *Mathematical Methods in the Applied Sciences, 42* (2018), 16, pp. 5258-5265
[16] Alkan, S., Secer, A., Solution of Non-linear Fractional Boundary Value Problems with Non-homogeneous Boundary Conditions, *Applied and Computational Mathematics, 14* (2015), 3, pp. 284-295

Paper submitted: December 30, 2022
Paper revised: February 5, 2023
Paper accepted: June 10, 2023